Effect of a titania covering on CNTS as support for the Ru catalysed selective ┬ CO methanation

David O. Kumi[a], Tumelo N. Phaahlamohlaka[a], Mbongiseni W. Dlamini[a], Ian T. Mangezvo[a], Sabelo D. Mhlanga[b], Michael S. Scurrell[c,], Neil J. Coville[a,]

[a] Molecular Sciences Institute, School of Chemistry, University of the Witwatersrand, Johannesburg, South Africa
[b] Nanotechnology and Water Sustainability Research Unit, College of Science, Engineering and Technology, University of South, Florida, 1709, Johannesburg, South Africa
[c] Department of Civil and Chemical Engineering, University of South Africa, Florida, 1710, Johannesburg, South Africa

ARTICLE INFO

Keywords:
Carbon nanotubes
Nitrogen dope
TiO_2 coating
CO methanation

ABSTRACT

One of the major set-backs in the selective CO methanation process, as the final clean-up step in removing residual CO from reformate gas feed, is the reverse water gas shift (RWGS) reaction. This reaction is an undesired reaction because, it runs parallel with the selective CO methanation reaction. This increases the CO outlet concentration. The catalytic performance of ruthenium supported on carbon nanotubes (CNTs), nitrogen doped carbon nanotubes (NCNTs), titania coated carbon nanotubes (NCNT-TiO_2 and CNTs-TiO_2) and TiO_2 anatase (TiO_2-A) for selective CO methanation was investigated. The feed composition relevant to reformate gas was used but in the absence of steam. The experiments were conducted within a temperature range of 100 °C and 360 °C. It was observed that carbon dioxide methanation was suppressed until CO methanation attained a maximum conversion for all the catalysts studied. The Ru/NCNT showed higher activity than Ru/CNT at all temperatures examined due to the nitrogen incorporation in the carbon domains. Both Ru/CNT and Ru/NCNT however promoted the RWGS reaction at temperatures above 250 °C. The Ru/CNT-TiO_2 catalyst recorded the highest activity for both the CO and selective CO methanation followed by Ru/TiO_2-A. The presence of titania on the carbon nanotubes significantly retarded the RWGS reaction from about −120% CO conversion to about 80% CO conversion, while selectivity towards methane increased in all catalysts with increasing temperature.

1. Introduction

Numerous efforts to fine tune the proton exchange membrane fuel cell (PEMFC) technology have been reasonably successful, especially as relates to the transportation industry which uses electrical power sources. This would apply to both stationary fuel cell applications and portable fuel cells. One of the major setbacks hindering possible com-mercialisation of a low temperature PEMFC is the generation of a "nearly-CO-free" gas feed but the current processes use may leave re-sidual quantities of CO in the H_2 rich feed [1]. Hydrogen rich fuels for PEMFCs are obtained by reforming hydrocarbons, e.g. liquefied petro-leum and natural gas [1–3]. Trace amounts of CO impurities can de-activate the anode electrode of a PEMFC. For example, the anode electrocatalyst composed of Pt-Ru only tolerates a <50 ppm CO con-centration [4–6], while a Pt anode electrocatalyst can only tolerate concentrations of <10 ppm [7–9].

Usually, the water gas shift (WGSR) reaction is employed in initial process for clean-up when the CO concentration is in the range of 1–8%. Thus secondary processes are needed to reduce the CO level to ppm levels after the initial process.

There are several techniques that have been used to reduce CO in a reformate gas feed to lower concentrations, for use in a PEMFC [10]. These include using pressure swing adsorption (PSA), a method that makes use of special adsorptive materials (e.g. zeolites), which are employed as molecular sieves. The preferential CO oxidation (PROX) reaction Eq. (3) has also been widely studied over the years but today much focus has shifted from PROX to selective CO methanation called SMET (Eq. (1)) as a technique for removal of the final traces of CO in reformate gas feed. This is because SMET can avoid the limitations experienced by PROX such as addition of air from an external source. The CO and CO_2 methanation reactions (as indicated in Eqs. (1) and (2)) are less exothermic than the CO and H_2 oxidation reactions (Eqs. (3) and (4)), which makes it inherently easier to control SMET than PROX.

$$CO + 3H_2 \leftrightarrow CH_4 + H_2O \qquad \Delta H^{\circ}298 = -206\ kJ/mol \qquad (1)$$

Corresponding authors.
E-mail addresses: scurrms@unisa.ac.za (M.S. Scurrell), Neil.Coville@wits.ac.za (N.J. Coville).

$$CO + 4H_2 \leftrightarrow CH_4 + 2H_2O \qquad \Delta H^{\circ}298 = -165\ kJ/mol \qquad (2)$$

$$CO + (½)O_2 \leftrightarrow CO_2 \qquad \Delta H^{\circ}298 = -284\ kJ/mol \qquad (3)$$

$$H_2 + (½)O_2 \leftrightarrow H_2O \qquad \Delta H^{\circ}298 = -244\ kJ/mol \qquad (4)$$

$$CO_2 + H_2 \rightarrow CO + H_2O \qquad \Delta H^{\circ}298 = 41\ kJ/mol \qquad (5)$$

The SMET process is considered as a most promising process to remove CO in a reformate gas stream for PEMFC applications. The key to development in SMET is the design of an efficient catalyst, capable of removing CO, retarding CO_2 and inhibiting the RWGS reaction (Eq. (5)) at a sufficiently low temperature. Otherwise the methanation of carbon dioxide would occur which would then be a major hydrogen-consuming reaction.

A number of catalysts have been tested for this methanation of CO. They include Rh [11–14], Ni [12,15,16] and Ru [14,17,18]. In the selective CO methanation reaction Ru and Rh are still considered to yield high activities and unlike Pt and Pd do not promote the undesired reverse water gas shift reaction [19]. The nature of the support plays a role in the overall performance of a catalyst and this suggests a strategy to modify the behaviour of SMET catalysts [13,20,21].

Recently the use of carbon nanotubes (CNTs) as model catalyst supports for hydrogenation reactions such as the Fischer-Tropsch (FT) reaction has increased. CNTs have become attractive due a number of advantages they possess such as facile modification of their surface properties, good hydrothermal stability and above all, their moderate interaction with the active metal [22]. The impressive mechanical nature of carbon supports and the absence of micro-porosity, which reduces intraparticle mass transfer in reaction media, as well as the easy accessibility of the active metal phases makes the CNT an excellent catalyst support.

Carbon supports do however have a very low density which is a problem in terms of using the CNTs in commercial reactors. Other types of supports, for example the metal oxides such as TiO_2, SiO_2 and Al_2O_3 can be used but they suffer from strong metal support interactions and even the formation of mixed metal compounds in some cases or spinel. Carbon does not experience spinel or possibly no strong metal support interactions.

Combining carbon and titania, could improve or merge the properties of both the carbon and oxide supports. The photocatalytic abilities of TiO_2 are known to be enhanced by doping or coating titania with carbon. The position that carbon occupies in a TiO_2 matrix will determine its effect on the carbon [23]. Since the density of carbon materials is enhanced by coating carbon with TiO_2 (or vice versa) [24] these methodologies suggests a process for increasing the catalyst/support density when C is used in the support.

In this paper we report on the enhanced catalytic activity and suppression of the RWGS reaction using Ru as the active metal phase supported on TiO_2 coated CNTs. A simple hydrothermal route was employed to coat the CNTs with TiO_2.

2. Experimental

2.1. The synthesis of CNTs

CNTs and nitrogen doped CNTs (N-CNTs) were synthesized by using the chemical vapour deposition (CVD) technique [25]. The CNTs and N-CNTs were grown using a 5%Fe-5%Co/$CaCO_3$ catalyst [25,26]. About 1 g catalyst was placed in a quartz boat and placed in the middle of a quartz tube in a furnace. The furnace was heated to 700 °C at a rate of 10 °C per minute under a nitrogen flow rate of 240 ml/min. Once the reaction temperature was attained, acetylene gas was introduced into the reaction chamber at a flow rate of 90 ml/min. The reaction was then allowed to continue for 1 h. After the reaction, the acetylene gas flow was stopped and the reactor was allowed to cool to room temperature under a flow of nitrogen gas. For the N-CNT synthesis, acetylene was bubbled through acetonitrile (acetonitrile the source of nitrogen) [26], and the CH_3CN/C_2H_2 introduced into the CVD reactor.

The CNTs were washed with 55% HNO_3 to remove both residues of the catalyst and to functionalise the CNTs at the same time. To do this, a concentrated solution of 55% HNO_3 was added to the as-synthesised CNTs or the N-CNTs in a round bottom flask. The mixture was then refluxed at 110 °C for a period of 12 h. The residue was washed with a large amount of deionised water till the solution had a neutral pH. The CNTs were collected by filtration and then dried overnight in an oven at 100 °C.

2.2. Synthesis of CNT-TiO_2 composites and TiO_2 anatase

CNT-TiO_2 was synthesized by modifying the procedure used by Yan et al. [27]. In a typical synthesis, 1.0 g of CNTs were dispersed in 30 ml of butanol and sonicated for 30 min. Titanium butoxide was dissolved separately in 10 mL butanol, sonicated for 20 min and then added dropwise to the functionalised CNTs while stirring at a temperature of 30 °C. Diethylamine (0.6 ml) was added dropwise to the above mixture which was stirred for 10 min at room temperature to catalyse Ti-O-Ti formation reactions. The mixture was then transferred into a Teflon lined autoclave and the reaction was carried out at 150 °C for 14 h. The product was centrifuged, washed several times with ethanol followed by water and then calcined at 250 °C for 4 h under nitrogen. The same procedure was repeated without any CNTs to synthesise titania with an anatase polymorph. This support was denoted as TiO_2-A.

2.3. Preparation of the catalyst by wet impregnation

The catalysts were prepared by using $RuCl_3$ as metal precursor. Approximately 1.74 mL of $RuCl_3$ solution was dissolved in 10 mL of deionised water and then sonicated for 15 min. The $RuCl_3$ solution was then added drop-wise into a beaker containing 1 g of the support (CNT, N-CNT, TiO_2 or CNT-TiO_2). The thick paste formed was dried in an oven overnight and then calcined at 250°C for 3 h to remove unwanted residues.

2.4. Catalyst activity studies

Catalyst performance was tested in a fixed-bed tubular reactor (FBTR) of height 250 mm and an internal diameter of 16 mm. The reaction was carried out at atmospheric pressure. The temperature of the reaction was measured in the catalyst bed using a K-type thermocouple. For each run, 1 g of the catalyst was weighed and placed in a reactor. Prior to the reactions, the catalyst was reduced at 250 °C for 4 h at 1 bar pressure under 99.995% H_2 gas. The various reactions (CO methanation, CO_2 methanation and selective CO methanation in the presence of CO_2) were investigated in the temperature range 160–360 °C using a gas feed with composition of 1% CO, 20% CO_2, 10% N_2 and H_2 balance. A flow rate of 90 ml/min was used to feed the gas feed to the reactor. Online GCs were connected to the FBTR to monitor the reaction. Both a flame ionization detector (FID) and a thermal conductivity detector (TCD) were used.

2.5. Characterization

The surface areas of all the catalysts and supports were analysed by BET using N_2 physisorption (Micromeritics ASAP-2000 Tri-star analyser). Before the surface area analysis, 0.2 g of the sample was degassed for 6 h at 150 °C under a N_2 flow using a Micromeritics flow Prep 060. The weight losses of the carbon samples were monitored on a Perkin-Elmer STA6000 TG/DTA Thermogravimetric analyser. The analyses were performed in air at a heating rate of 10 °C/min. Powder X-ray diffraction (XRD) studies were done on a Siemens D2 diffractometer using Co Kα radiation equipped with a Ni filter. Steps of 0.02° with a scan range of 10–90° were used. The morphologies of the

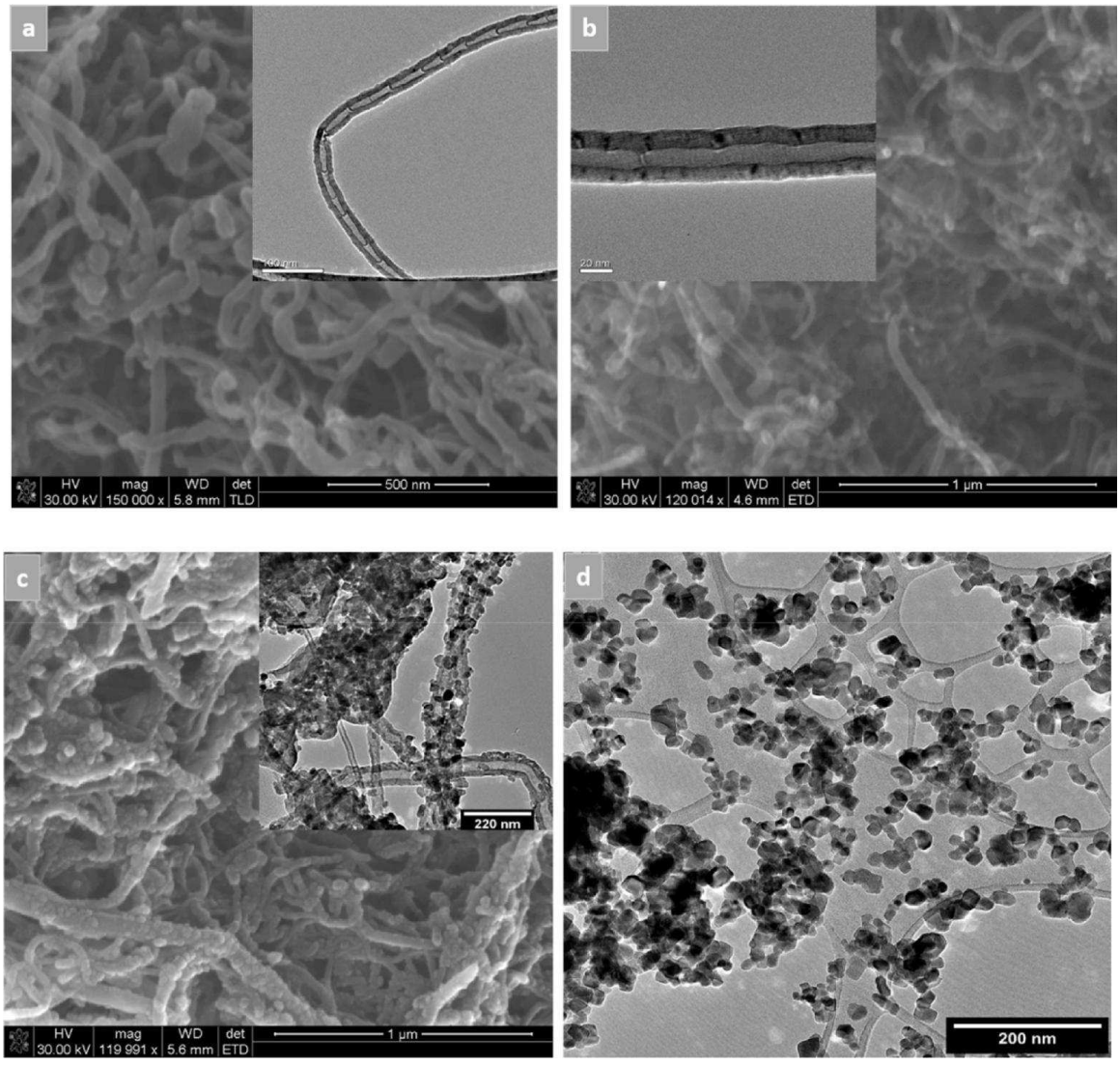

Fig. 1. Images of the different supports synthesised: (a) SEM and TEM image of N-CNTs, (b) SEM and TEM image of CNTs, (c) SEM and TEM image of CNT-TiO_2 and (d) TEM image of TiO_2.

samples were identified using SEM (FEI Nova Nanolab 600) and TEM (Tecnai T12) images. TEM samples were prepared by dissolving the catalyst in ethanol followed by sonication for 2 min. A drop of the ethanol suspension was transferred to a copper grid and dried. The disorder in the carbon based supports was measured with a micro-Raman attachment of a Jobin-Yvon T64000 Raman spectrometer. The excitation wavelength used was 514.5 nm from an Ar ion laser and the spot size on the sample was ca. 1.5 µ in diameter.

3. Results and discussion

3.1. Support characterization

3.1.1. TEM and SEM analysis

TEM analysis was used to elucidate the structural and morpholo-gical features of the different supports. From the images (both SEM and TEM) shown in Fig. 1, the expected tubular structure for the CNTs and N-CNTs was observed. Incorporation of nitrogen in the CNT's is usually characterized by the presence of bamboo like structures, which are typically seen as a series of compartments inside the tube. The TEM insert of Fig. 1a shows this structure. Both CNTs and N-CNTs were identified to be multi-walled. Their diameters were found to be in the range of 40–70 nm and 30–80 nm for CNTs and N-CNTs respectively.

Analysis carried out to quantify the nitrogen content present in the N-CNTs was found to be 3.7% by mass using CHNS analysis. This was confirmed with the presence of the bamboo structure seen in the TEM image. Fig. 1c shows the SEM and TEM images of the CNTs coated with TiO_2. A closer view of the TEM image (insert in Fig. 1c; higher re-solution image) showed that the coverage of the TiO_2 was not complete on the CNTs. There were some regions with little coating and other regions where the titania nanoparticles formed aggregates along the length of a carbon nanotube. The anatase coating on N-CNT (NCNT-TiO_2) produced smaller TiO_2 particles and these covered the NCNTs (Fig. S1) more than observed for the CNT-TiO_2 sample. This could be due to the presence of surface nitrogen.

3.1.2. Raman spectral analysis

Raman spectroscopy was used to determine the crystallinity and information on the defects in the synthesised CNTs and N-CNTs. Two main characteristic peaks are associated with carbonaceous materials. These peaks are the D-band (approximately 1350–1360 cm^{-1}) which identifies with the defects, while the G-band (1590–1600 cm^{-1}) cor-responds to the CeC bond stretching mode in the graphite plane. The area ratio of the Ge to De bands (I_D/I_G) gives an idea of the extent of defects in the carbon material. A high ratio suggests high levels of de-fects [28]. The Raman spectrum (Fig. 2) showed that nitrogen

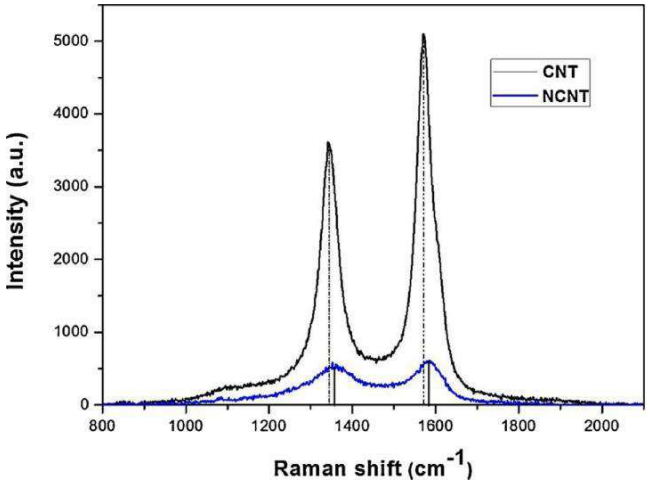

Fig. 2. Raman spectra of the in CNTs and N-CNTs.

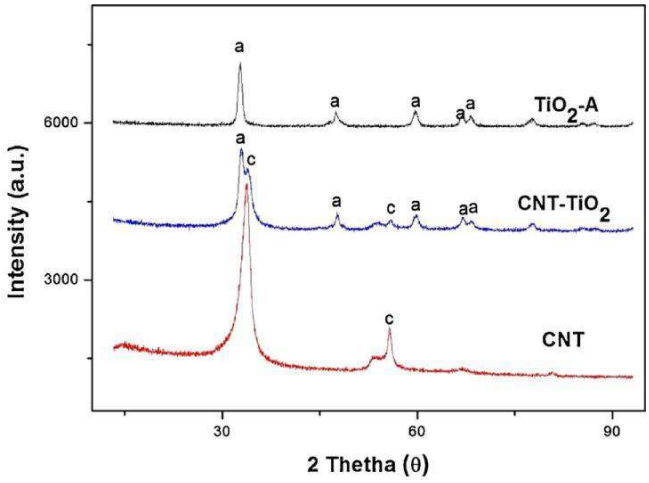

Fig. 3. PXRD pattern of supports: CNT, CNT-TiO_2 and TiO_2-A.

Table 1
Physiochemical properties of the supports and Ru catalysts.

	Sample				
	CNT	NCNT	CNT-TiO_2	N-CNT-TiO_2	TiO_2
Support					
BET surface area (m^2/g)	75	91	119	121	52
Pore volume area (cm^3/g)	0.22	0.31	0.38	0.29	0.21
D-band (cm^{-1})	1344	1357	–	–	–
G-band (cm^{-1})	1571	1583	–	–	–
I_D/I_G ratio	0.70	0.85	–	–	–
Decomposition Temperature (°C)	591	433	615	514	–
Catalyst					
BET surface area (m^2/g)	66	71	108	116	41
Pore volume area (cm^3/g)	0.25	0.41	0.35	0.31	0.23
$d_{RuO2TEM}$	6.4	3.8	2.3	–	3.6
$d_{RuO2XRD}$	7.9	4.6	–	–	4.2
Ru dispersion (%)	23	38	52	50	38

incorporation into the CNTs increased the defect concentration as seen by the increased I_D/I_G ratio (Table 1). The broadening of the D and Ge bands coupled with a slight shift to higher wave numbers again con-firmed an increased defect concentration in the N-CNTs [29]. Usually, defects result in the creation of anchorage sites for nano metal particles which serve as the active species in catalysis.

3.1.3. PXRD analysis

The crystalline phases in the support materials were identified by PXRD. As shown in Fig. 3, graphite carbon peaks at 2θ angles of ca. 31° were present in all the carbon containing supports (N-CNTs not shown). The diffraction patterns for the hydrothermally produced TiO_2 and the TiO_2 coated CNTs (NCNT-TiO_2 similar to the CNT-TiO_2) corresponded to the anatase polymorph of TiO_2. The peaks obtained were similarly sharper as the pure anatase which indicates that the titania and carbon nanotubes were crystalline.

3.1.4. Thermogravimetric analysis (TGA)

The TGA plots in Fig. 4 allows for the determination of the per-centage purity and the thermal stability of the CNTs, N-CNTs and the coated CNTs. The TGA plots of the unpurified samples (as-synthesised CNTs and N-CNTs) are shown in Fig. S2. It is noted that the HNO_3 acid treatment was effective in removing the bulk of the residue of the Fe and Co catalyst. The functionalization process significantly removed impurities (residue from catalyst) from about 30% < 1.5% and from 45% to < 2% for CNTs and N-CNTs respectively (Fig. S2). There were no weight loss registered below 400 °C which suggested that there was no

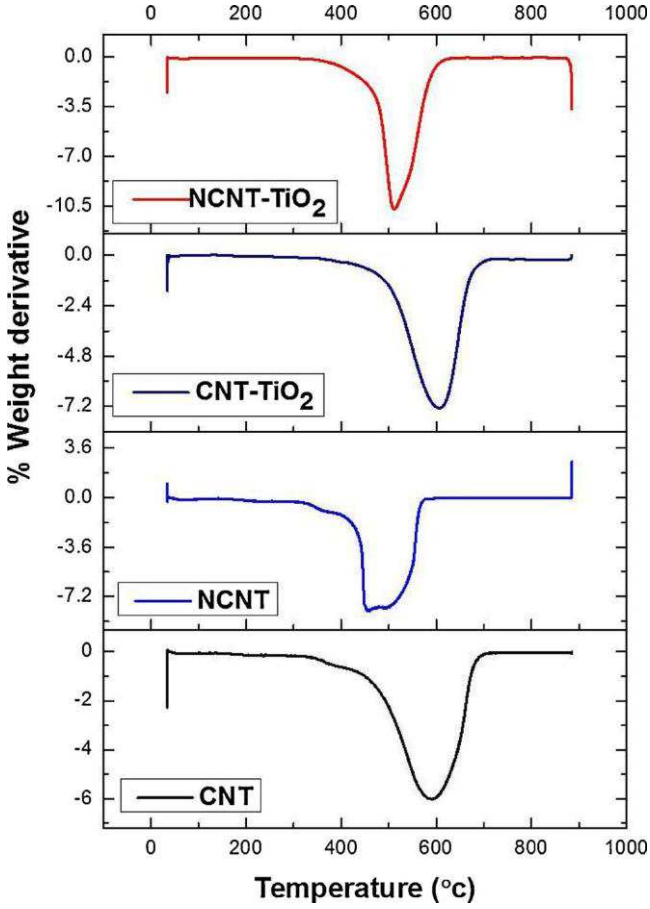

Fig. 4. TGA derivative profile showing CNT, NCNT, NCNT-TiO_2 and CNT-TiO_2.

amorphous carbon present [30,31]. The N-CNTs decomposed below 500 °C i.e. about 100 °C less than the CNTs. This is also an indication that presence of defects present in the carbon framework reducing the thermal stability of the carbon.

The TGA results also showed a small weight loss in the low tem-perature region of Fig. 4; this is due to the decomposition of butanol, diethylamine or other residual organic materials that were adsorbed onto/into the CNTs. The maximum decomposition temperature for the CNT-TiO_2 was around 63 °C, relatively higher than that for the CNTs. The TGA data indicated that about 25% of the CNT-TiO_2 was composed of TiO_2 (Fig. S2). The improvement in the thermal stability was as a

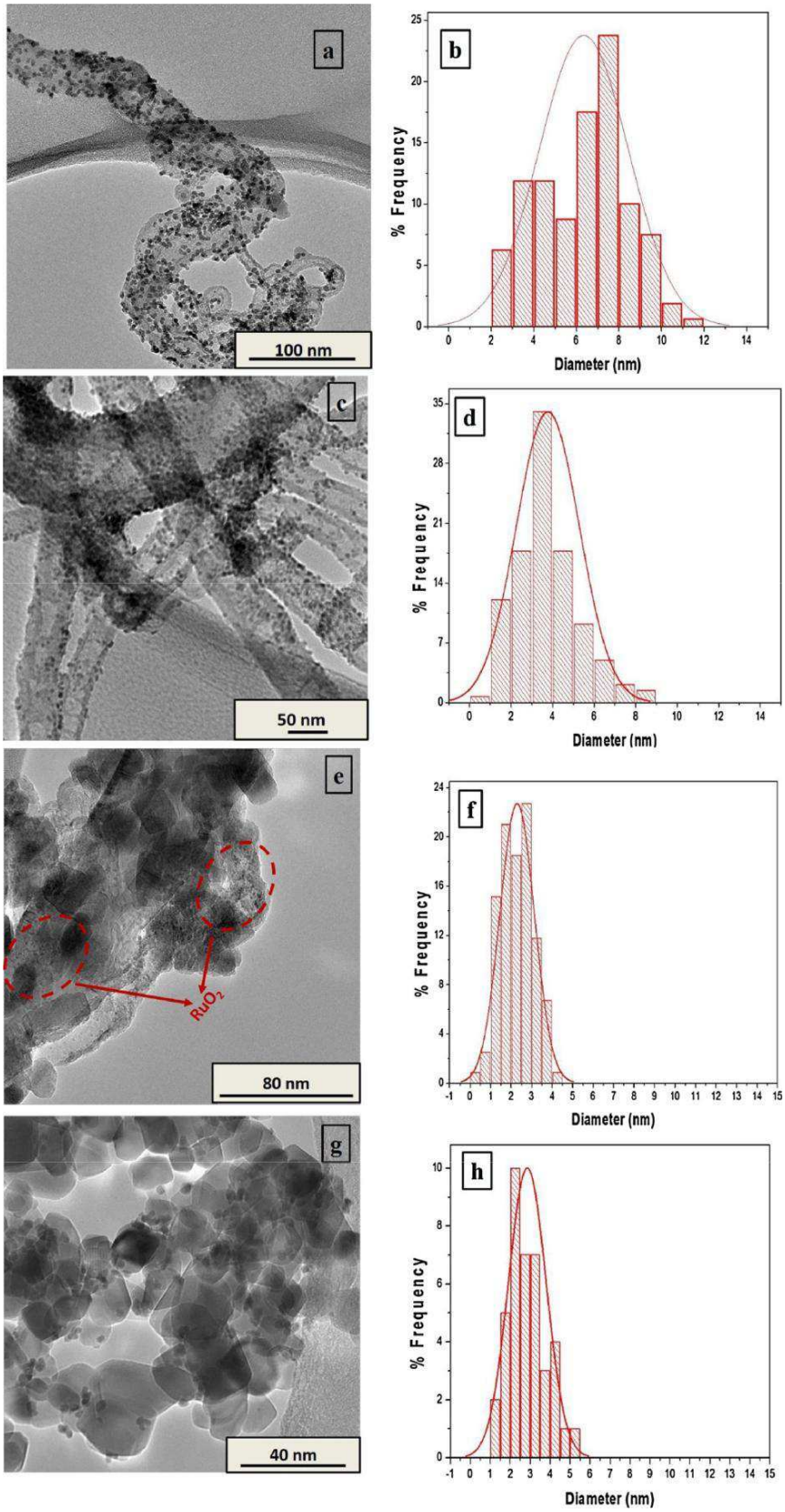

Fig. 5. Representative images showing RuO2 particles (and their size distribution) dispersed on the different supports: (a) TEM image of 5%Ru/CNT, (b) particle size distribution diagram for 5%Ru/CNT (c) TEM image of 5%Ru/N-CNT, (d) particle size distribution diagram for 5%Ru/N-CNT (e) TEM image of5%Ru/CNT-TiO_2 and (f) particle size distribution diagram for 5%Ru/CNT-TiO_2 (g) TEM image of 5%Ru/TiO_2 (h) particle size distribution diagram for 5%Ru/TiO_2.

result of the TiO_2 covering which shielded the carbon from oxidation.

3.1.5. N_2 adsorption studies

The surface area and porous structure of materials were determined using the nitrogen adsorption technique [32]. Introduction of nitrogen into the carbon matrix increased the surface area and increased the pore volume of the CNTs. This was attributed to both the functionalization process and the doping [25,29]. The hydrothermally produced anatase TiO_2 had the lowest surface area (52 m^2/g) which correlated with lit-erature data. Combining CNT with TiO_2 to form a CNT-TiO_2 composite significantly improved the surface area (from 75 and 52 to 119 m^2/g).

3.2. Catalyst characterization

3.2.1. TEM analysis on the catalyst

TEM images of the various catalysts prepared and studied are pre-sented in Fig. 5. The darker spots observed in all the TEM images are due to RuO_2 nano particles. The average RuO_2 particle size distribution calculated from the TEM images are shown in the size distribution plots. The RuO_2 particles on the CNT were observed to have an average size of 6.4 nm and to have a wider size distribution range compared to the other catalysts (Fig. 5b). The RuO_2 particle sizes on the N-CNTs were smaller with an average size of 3.8 nm (Table 1) with a relatively narrower size distribution (Fig. 5d). The presence of the nitrogen en-hanced anchoring of the RuO_2 particles [33]. The Ru supported CNT-TiO_2 particles were smaller (2.3 nm) than those found on the pure anatase TiO_2 support which also had fairly small RuO_2 particles (3.6 nm). This was probably due to the synergetic effect offered by the CNT-TiO_2 composite and the larger surface area. The Ru particles were distributed on both TiO_2 and the CNT surfaces as show in the TEM images.

3.2.2. BET analysis on the catalyst

The surface areas of the catalysts decreased compared to the sup-ports (Table 1). This was due to the occupation of the pores of the supports by Ru, particles. The pore volume increased slightly due to occupation of smaller pores after loading of the Ru except for the 5% Ru/CNT-TiO_2 sample [34].

3.2.3. PXRD analysis on the catalyst

The phases present in the Ru catalysts on the support were in-vestigated by XRD and are presented in Fig. 6. The peaks observed at 32.5 and 40.8 2θ were indexed to RuO_2 (110) and (101) planes re-spectively. No peaks for Ru were observed on 5%Ru/CNT-TiO_2 and 5% Ru/NCNT-TiO_2 (Fig. S2). This was due to the small undetected RuO_2 particles which were well dispersed as observed on the TEM analysis

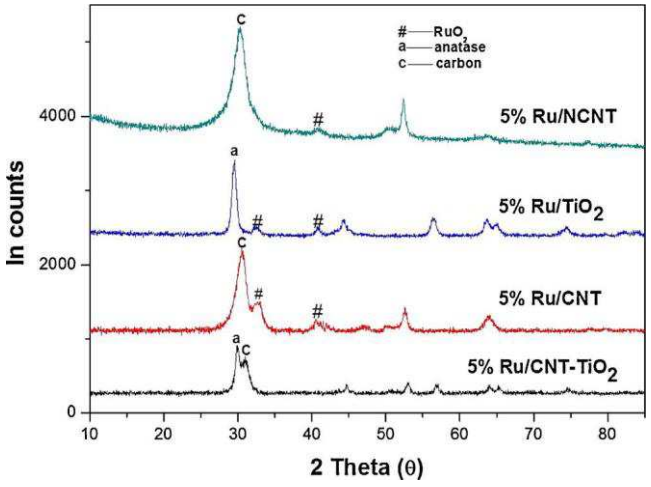

Fig. 6. PXRD patterns of the catalysts showing the RuO_2 crystalline phases.

and also the difficulty of observing Ru on TiO_2. The RuO_2 peaks ob-served on the CNT sample indicated larger particle sizes (7.9 nm from XRD, Table 1). The RuO_2 peaks for 5%Ru/N-CNTs and 5%Ru/TiO_2-A were almost similar (broad and less intense) which confirmed the re-latively smaller particles observed by TEM analysis.

3.2.4. TPR studies

The reduction profiles of the different catalysts are shown in the H_2-TPR plots in Fig. 7. Reduction of RuO_2 to Ru for all the catalyst occurred below 200 °C. The reduction profile for the carbon and titania compo-site revealed maximum broad reduction peaks at elevated temperatures 163 °C and 174 °C Ru/CNT-TiO_2 and Ru/N-CNT-TiO_2 respectively. This suggested Ru particles were dispersed on both the CNTs and TiO_2 components of the composites as observed in the TEM images. The broadness was attributed to RuO_2 reduction on the different support (carbon and titania supports). The RuO_2 particles were believed to have interacted slightly more strongly with the functional groups present on the carbon supports. This was revealed by the reduction RuO_2 to Ru occurring at relatively higher temperature compared to TiO_2-A sup-ported catalyst. Reduction on the N-CNTs (RuO_2 to Ru) occurred at slightly higher temperature than the RuO_2 on CNTs. This could be due to the extra lone pair of electron made available by the surface nitrogen (pyridinic nitrogen) which formed a stronger bond with the RuO_2 i.e. the nitrogen on the surface provided strong anchorage to Ru particles. Surprisingly, the RuO_2 supported on the TiO_2-A reduced at un-expectedly lower temperature (113 °C than both CNT and N-CNTs supports. To confirm this reduction observed on the anatase TiO_2, a series of anatase supports were synthesised using a sol gel method and a resin gel method and used as a Ru catalyst support. Their reduction profiles were compared to Degussa P25 TiO_2 Ru supported catalyst as shown in the Fig. S3. This may suggest that the CNTs and N-CNTs binds the Ru particles firmly through the functional groups or alternatively,

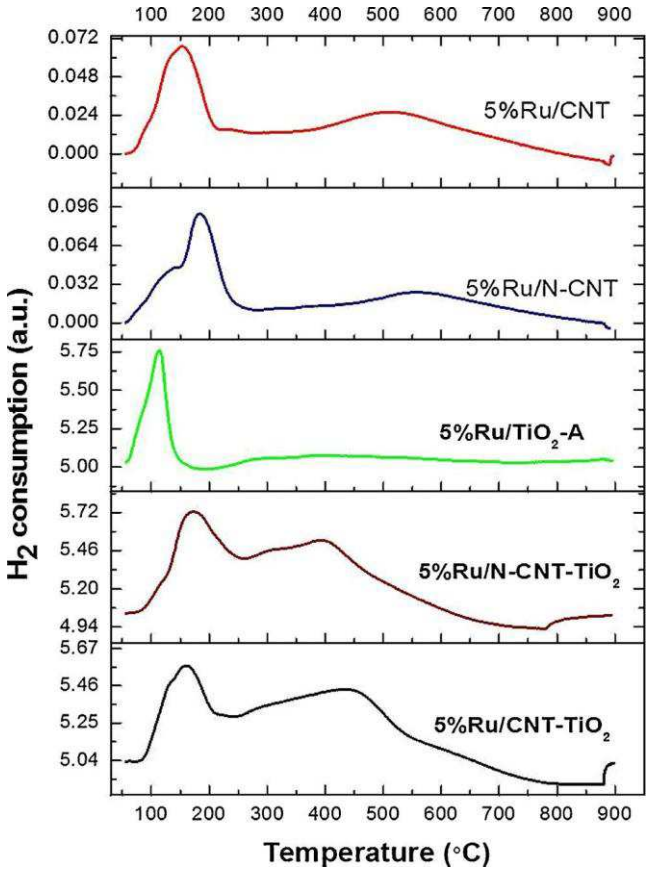

Fig. 7. H_2-TPR for the different catalyst.

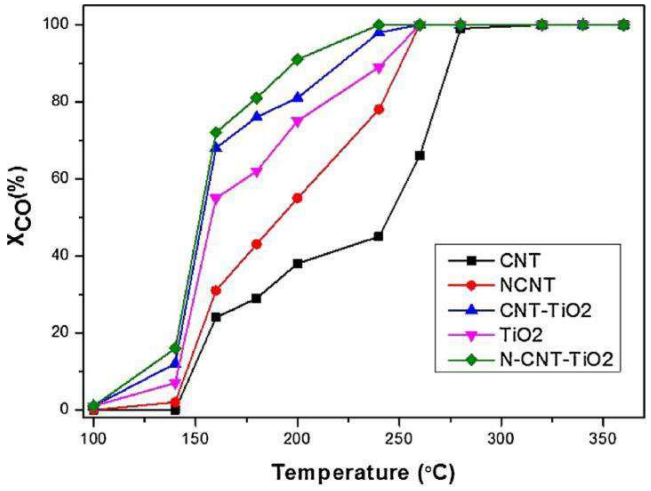

Fig. 8. The effect of the support on the catalytic performance of the CO con-versions (XCO) as function of reaction temperature using 5% wt.% Ru sup-ported catalyst. Experimental conditions: mass of catalyst: 1 g; reactant com-position: (a) 1% CO, 10% N_2 (balance H_2); total flow rate: 90 cm^3/min.

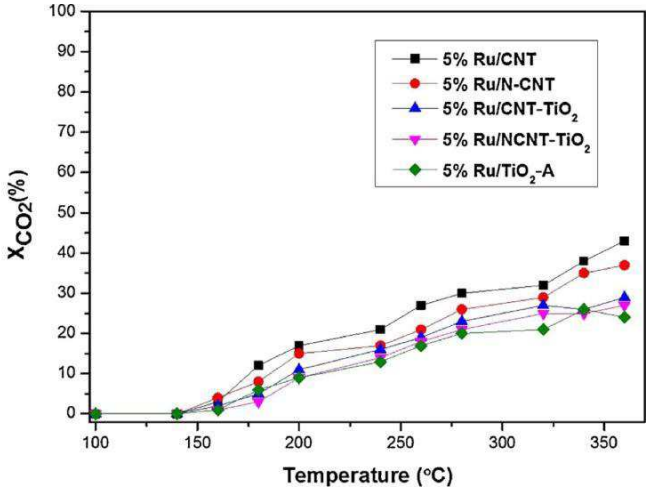

Fig. 9. The effect of the support on the catalytic performance of CO_2 conver-sions (XCO_2) as a function of reaction temperature using 5% wt.% Ru supported catalyst. Experimental conditions: mass of catalyst: 1 g; reactant composition: 20% CO_2, 10% N_2 (balance H_2); total flow rate: 90 cm_3/min.

the density (catalyst bed height) of the Ru/CNT and Ru/N-CNT con-tributed in a longer interaction of the hydrogen (reducing gas) which resulted in the shift in RuO_2 reduction peaks. This possibly affected the composite graphs. Further studies should be conducted (as stated in the recommendations) on TPR to clarify this.

The methanation or gasification of the carbon support was the reason assigned to the peaks occurring at higher temperatures. This peak was absent on the Ru/TiO_2-A profile.

4. CO hydrogenation

The activity and selectivity performance of the different supports (CNTs, NCNT, CNT-TiO_2 and TiO_2-A) for CO hydrogenation over Ru catalyst with performed with the same Ru loading (5 wt.%). The reac-tions were performed using CO or CO/CO_2 to study methanation and selective CO methanation conversion in the presence of CO_2. Fig. 8 summarizes the conversion data when only CO was used. Above ca.140 °C, all the catalysts investigated showed a steady increase in CO conversion (Fig. 8) and all attained 100% conversion at temperatures beyond 280 °C. The N-CNT Ru supported catalyst showed a higher ac-tivity than observed when CNT was used as a support. This was at-tributed to the presence of pyridinic nitrogen with an extra lone pair of electron which contributed extra electrons making the surface of the tubes more electronegative. This resulted in increased nucleation sites which served as anchorage sites thereby enhancing dispersion of the active phase while restricting the Ru particle sizes [33]. Again, the extra electrons due to the incorporation of nitrogen atom increased the electron density around the Ru and the electrons were then back do-nated from Ru d-orbitals to a π^* antibonding molecular orbital of CO. This strengthened the RueC bonds (back bonding) weakening the CeO bonding, promoting the dissociation of CO and increasing the metha-nation of CO with Ru/N-CNT over Ru/CNT [35]. It should be noted that, titania coating on the carbon nanotube as support exhibited the highest activity, performing better than Ru/TiO_2-A. This was due to the higher specific surface area of the coated support and the smaller par-ticle sizes of the Ru.

Anatase on its own has a high surface energy which tends to facil-itate agglomeration of metal particles supported on it [36–38]. Defects on titania surfaces (Ti^{3+} are related to anionic oxygen) which are known to be stabilize of metallic species from agglomerating [37], These Ti^{3+} surface defects are mostly associated with anatase-rutile transformation but Kongkiat et al. reported they could modify the surface structure (Ti^{3+} defects) of anatase by using varying oxygen content in their calcination process under temperatures below the anatse-rutile transformation [39]. These defects could have been in-troduced on the surface of our coated CNTs due to the presence of oxygen (made available through functionalizing the CNTs) present during the synthesis or calcination process. Alternatively, the small Ru particles found on the coated support may have resulted from syner-getic effects between the CNT-TiO_2 which is believed to have improved the specific surface area. The NCNT-TiO_2 performed slightly better than the CNT-TiO_2 composite. It can be concluded that the activity of CO hydrogenation is dependent on the type of support used in out ex-periments.

In spite of the small surface area recorded for the TiO_2-A support, the Ru catalyst showed much higher activity than the Ru/NCNT and Ru/CNT catalysts. Besides the presence of anionic vacancies that are present at the edges of the oxide-metal boundaries on the TiO_2, a complex is formed between the oxygen groups on the TiO_2 and the adsorbed CO [40]. Sachler and Ichikawa and co-authors suggested that the Lewis acid/base bonding interaction that occurs between the ad-sorbed CO and oxygen end and a promoter influence at the oxide/active metal interface [41,42]. These effects are said to enhance the cleavage of the C–O bond which results in higher activity for TiO_2.

4.1. CO_2 Hydrogenation

The hydrogenation of CO_2 was initiated above ca 150 °C as shown in Fig. 9. Conversion remained below 20% until 325 °C for all catalyst except Ru/CNT. It should be noted that no significant conversion oc-curred within the temperature window in which our catalysts were tested. This means significant methanation of CO_2 (above 50% con-version) may only occur at higher temperatures. The supports 5%Ru/ CNT and 5%Ru/N-CNT had higher activity than the other catalysts, and suggested the supports had effects on the CO_2 conversion. Several studies acknowledge that CO_2 mostly adsorbs on the supports while hydrogen is adsorbed on the metal to produce methane. The presence of OH groups could have contributed to the higher activity of the func-tionalized carbon supports [43]. The 5%Ru/CNT was slightly more active than 5%Ru/N-CNT, which could mean particle size played a role in the reaction.

5. Selective CO methanation

Fig. 10 summarises the performances of all the catalyst investigated for the selective methanation of CO in the presence of CO_2. The Figure

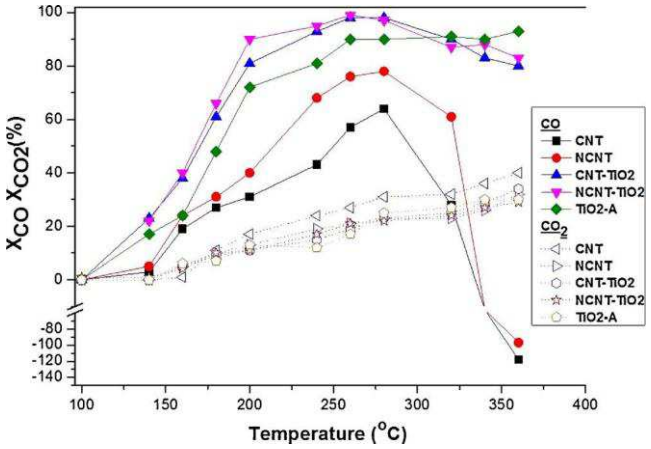

Fig. 10. The effect of the support on the catalytic performance of Ru the on selective methanation of CO in the presence of CO_2 ($X_{COX_{CO_2}}$) as a function of reaction temperature using 5% wt.% Ru. Solid symbols: CO conversion: open symbols: CO_2 conversion. Experimental conditions: mass of catalyst: 1 g; re-actant composition: 1% CO, 20% CO_2, 10% N_2 (balance H_2); total flow rate: 90 cm^3/min.

showed a similar activity sequence for all the catalysts performance as seen when only CO was hydrogenated. The same explanations can be given to the activity trend noted for the selective CO methanation re-action. CO conversion was initiated at about ca. 140 °C for all catalysts. The conversion of CO increased with increasing temperature for all the catalyst; at 280 °C, both Ru/CNT and Ru/N-CNT attained maximum conversions of 64% and 78% respectively. Increasing the temperature further above (>280 °C) indicated a drop in CO conversion revealing "negative" percentage values for CNT and N-CNT at about 320 °C. This is due to the CO hydrogenation reaction (Eq. (1)) running parallel to the RWGS reaction (Eq. (5)) under the experimental conditions. The "ne-gative" CO conversion showed that the effluent CO concentration drastically increased due a slower rate of CO hydrogenation compared to the rate at which CO was produced via the RWGS reaction. This behaviour implies that both CNT and N-CNT promoted the RWGS re-action. Although, a drop in CO conversion was observed for NCNT-TiO_2 and CNT-TiO_2 at ca. the same temperature, the effect is small. Clearly, the presence of anatase TiO_2 supressed the RWGS reaction relative to the Ru/N-CNTs and Ru/CNTs. This result is in agreement with the study by Jiménez et al. who used different carbon nanofibers; they observed that the carbon material promoted a high RWGS [19].

Hydrogenation of CO_2 in the presences CO was minimal at tem-peratures before CO attained maximum conversion for all the catalysts investigated. This confirms that CO interacted more strongly on the surface of the catalyst than CO_2, in agreement with reports by several authors [44–46]. It is widely accepted that CO_2 hydrogenation proceeds by the adsorption of CO_2 on the support with H_2 on the metal [47–50]. The work of Shohei et al. suggested that the presences of hydroxyl groups on TiO_2 at elevated temperatures facilitated the hydrogenation of CO_2 [43]. The CNT and N-CNT supports are known to have hydroxyl groups on the surface from the acid treatment. This could possibly ex-plain the relatively higher conversion of CO_2 on Ru/CNT.

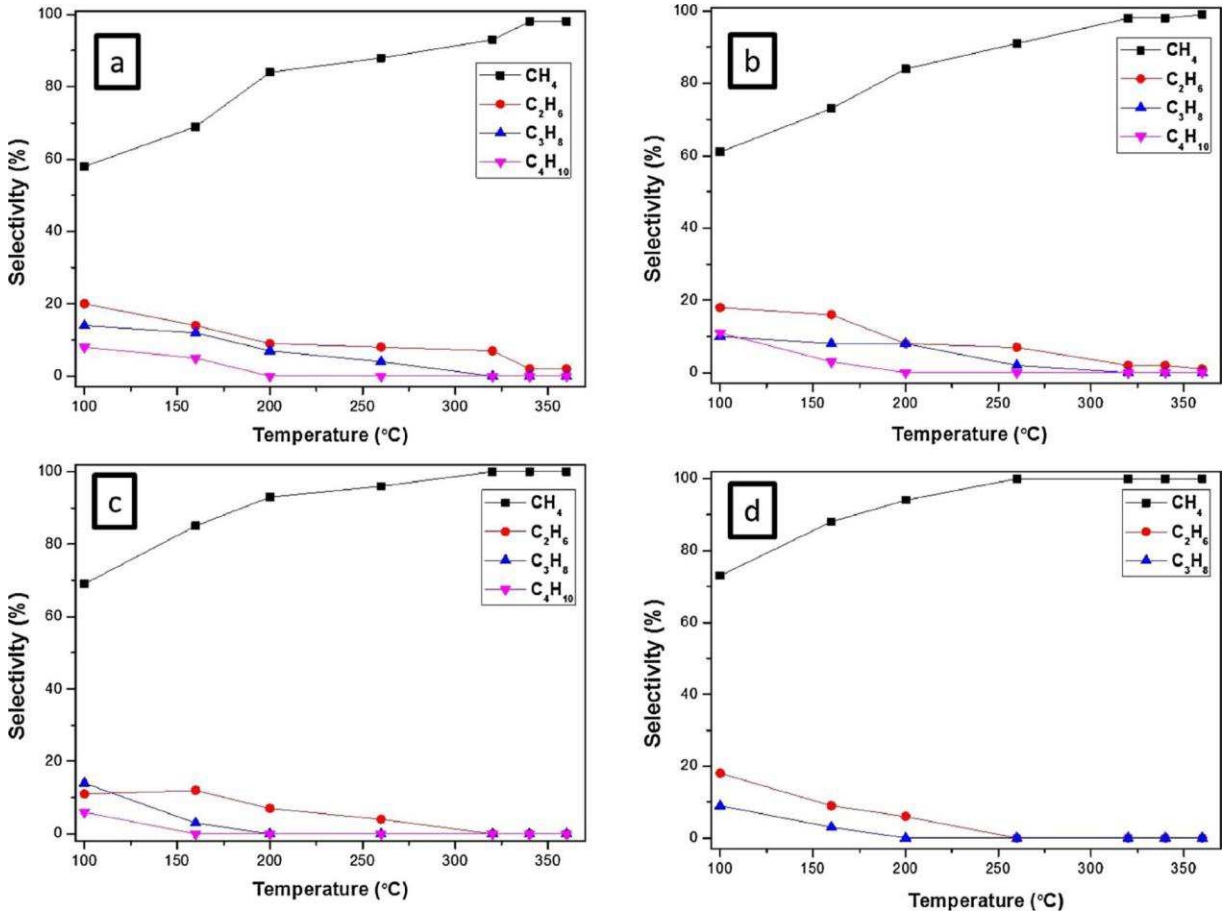

Fig. 11. The effect of reaction temperature on the selectivity of (a) 5%Ru/CNT (b) 5%Ru/N-CNT (c) 5%Ru/CNT-TiO_2 and (d) 5%Ru/TiO_2 catalysts during the selective CO hydrogenation.

6. Methane selectivity

Several studies that have focused on selective CO methanation have shown that besides methane other higher hydrocarbons are formed, especially at low temperatures when CO conversions are low. In our studies, plots revealed that besides methane, the hydrogenation of CO/ CO_2 resulted not only in methane but other higher hydrocarbons (Fig. 11). The catalyst supported on pure anatase (5%Ru/TiO_2-A) showed the highest selectivity towards methane. Fig. 10d shows that other than methane only C_2 and C_3 molecules were formed at low temperatures. Above 260 °C only methane was observed. The CNT-TiO_2 composite showed 100% methane selectivity at temperatures above 300 °C. Both 5%Ru/N-CNT and 5%Ru/CNT did not attain total methane selectivity in the temperature range of this study. The data show that larger Ru particle sizes support higher carbon growth. Similar results were observed for CNT-TiO_2 and NCNT-TiO_2 (not shown).

7. Conclusions

The coating of CNTs and N-CNTs using titania was successfully done. However, the coating did not result in total coverage. The coating of CNTs and N-CNTs with titania produced a catalyst support with better thermal stability and a larger surface area compared to the functionalised CNTs. The catalytic activity as well as selectivity in this study depended on the support used and experimental conditions used (e.g. only CO methanation, the mixture of CO and CO_2, reaction tem-perature etc.). Total CO conversion was attained for all catalysts at a temperature ca. 280 °C when only CO was methanated. In the presence of CO_2, a slight variation of conversions was recorded for all catalysts. The titania coated CNT showed significantly higher activity compared to the uncoated CNTs and N-CNTs. The presence of TiO_2 on the CNTs suppressed the RWGS reaction and the CO methanation rate. Higher temperatures increased methane selectivity at the expense of higher hydrocarbon formation.

Acknowledgments

The authors wish to thank the National Research Foundation (NRF) and the University of the Witwatersrand for financial support. Thanks are also given to Mr L Hlekelele and Dr T Lerotholi for their help in various aspects of this work.

Appendix A. Supplementary data

Supplementary material related to this article can be found, in the online version, at doi:https://doi.org/10.1016/j.apcatb.2018.02.016.

References

[1] A.N.J. Van Keulen, J.G. Reinkingh, (2002) Hydrogen purification, U.S. Patent No. 6, 403,049. 11 June.
[2] F. Mueller-Langer, E. Tzimas, M. Kaltschmitt, S. Peteves, Int. J. Hydrogen Energy 32 (2007) 3797–3810.
[3] L.L. Vasiliev, L.E. Kanonchik, A.G. Kulakov, D.A. Mishkinis, A.M. Safonova, N.K. Luneva, Int. J. Hydrogen Energy 32 (2007) 5015–5025.
[4] X. Cheng, Z. Shi, N. Glass, L. Zhang, J. Zhang, D. Song, Z.-S. Liu, H. Wang, J. Shen, J. Power Sources 165 (2007) 739–756.
[5] C. Farrell, C. Gardner, M. Ternan, J. Power Sources 171 (2007) 282–293.
[6] N. Fujiwara, K. Yasuda, T. Ioroi, Z. Siroma, Y. Miyazaki, Electrochim. Acta 47 (2002) 4079–4084.
[7] Y. Borodko, G. Somorjai, Appl. Catal. A 186 (1999) 355–362.
[8] J. Divisek, H.-F. Oetjen, V. Peinecke, V. Schmidt, U. Stimming, Electrochim. Acta 43 (1998) 3811–3815.
[9] E. Passalacqua, F. Lufrano, G. Squadrito, A. Patti, L. Giorgi, Electrochim. Acta 46 (2001) 799–805.
[10] D.L. Trimm, Z.I. Önsan, Catal. Rev. 43 (2001) 31–84.
[11] P. Panagiotopoulou, D.I. Kondarides, X.E. Verykios, Appl. Catal. A 344 (2008) 45–54.
[12] F. Solymosi, A. Erdöhelyi, J. Mol. Catal. 8 (1980) 471–474.
[13] F. Solymosi, A. Erdöhelyi, T. Bansagi, J. Catal. 68 (1981) 371–382.
[14] K. Xavier, R. Sreekala, K. Rashid, K. Yusuff, B. Sen, Catal. Today 49 (1999) 17–21.
[15] S.-I. Fujita, N. Takezawa, Chem. Eng. J. 68 (1997) 63–68.
[16] T. Inui, M. Funabiki, M. Suehiro, T. Sezume, J. Chem. Soc. Faraday Trans. 1 Phys. Chem. Condens. Phases 75 (1979) 787–802.
[17] A.E. Aksoylu, Z. İlsenÖnsan, Appl. Catal. A 164 (1997) 1–11.
[18] T. Van Herwijnen, H. Van Doesburg, W. De Jong, J. Catal. 28 (1973) 391–402.
[19] V. Jiménez, P. Sánchez, P. Panagiotopoulou, J.L. Valverde, A. Romero, Appl. Catal. A 390 (2010) 35–44.
[20] J. Bracey, R. Burch, J. Catal. 86 (1984) 384–391.
[21] S.Y. Wang, S. Moon, M.A. Vannice, J. Catal. 71 (1981) 167–174.
[22] H. Xiong, H.N. Pham, A.K. Datye, J. Catal. 302 (2013) 93–100.
[23] R. Leary, A. Westwood, Carbon 49 (2011) 741–772.
[24] C. Papo, Z. Tetana, P. Franklyn, S. Mhlanga, J. Mater. Res. 28 (2013) 440–448.
[25] S.D. Mhlanga, N.J. Coville, Diamond Relat. Mater. 17 (2008) 1489–1493.
[26] Z. Tetana, S. Mhlanga, G. Bepete, R. Krause, N. Coville, South Afr. J. Chem. 65 (2015) 39–49.
[27] Y. Yan, J. Lu, C. Deng, X. Zhang, Talanta 107 (2013) 30–35.
[28] G.F. Malgas, C.J. Arendse, N.P. Cele, F.R. Cummings, J. Mater. Sci. 43 (2008) 1020–1025.
[29] Z.N. Tetana, Boron and Nitrogen Doped Carbons for Photochemical Degradation Reactions, PhD Thesis, The University of the Witwatersrand, Johannesburg, 2013.
[30] B.J. Landi, C.D. Cress, C.M. Evans, R.P. Raffaelle, Chem. Mater. 17 (2005) 6819–6834.
[31] Z. Shi, Y. Lian, F.H. Liao, X. Zhou, Z. Gu, Y. Zhang, S. Iijima, H. Li, K.T. Yue, S.-L. Zhang, J. Phys. Chem. Solids 61 (2000) 1031–1036.
[32] G. Leofanti, M. Padovan, G. Tozzola, B. Venturelli, Catal. Today 41 (1998) 207–219.
[33] P. Ayala, R. Arenal, M. Rümmeli, A. Rubio, T. Pichler, Carbon 48 (2010) 575–586.
[34] N.S. Babu, N. Lingaiah, N. Pasha, J.V. Kumar, P.S. Prasad, Catal. Today 141 (2009) 120–124.
[35] R.D. Gonzalez, H. Miura, J. Catal. 77 (1982) 338–347.
[36] C. Di Valentin, G. Pacchioni, A. Selloni, J. Phys. Chem. C 113 (2009) 20543–20552.
[37] A. Nobile, M. Davis, J. Catal. 116 (1989) 383–398.
[38] T. Ohno, K. Sarukawa, K. Tokieda, M. Matsumura, J. Catal. 203 (2001) 82–86.
[39] K. Suriye, P. Praserthdam, B. Jongsomjit, Appl. Surf. Sci. 253 (2007) 3849–3855.
[40] A. Boffa, C. Lin, A. Bell, G. Somorjai, Catal. Lett. 27 (1994) 243–249.
[41] W.M. Sachtler, M. Ichikawa, J. Phys. Chem. 90 (1986) 4752–4758.
[42] W. Sachtler, D. Shriver, W. Hollenberg, A. Lang, J. Catal. 92 (1985) 429–431.
[43] S. Tada, R. Kikuchi, K. Urasaki, S. Satokawa, Appl. Catal. A 404 (2011) 149–154.
[44] M.B.I. Choudhury, S. Ahmed, M.A. Shalabi, T. Inui, Appl. Catal. A 314 (2006) 47–53.
[45] T. Inui, M. Funabiki, Y. Takegami, Ind. Eng. Chem. Prod. Res. Dev. 19 (1980) 385–388.
[46] P. Panagiotopoulou, D.I. Kondarides, X.E. Verykios, Appl. Catal. A 344 (2008) 45–54.
[47] A.E. Aksoylu, Z.I. Önsan, Appl. Catal. A 164 (1997) 1–11.
[48] N.M. Gupta, V.S. Kamble, V.B. Kartha, R.M. Iyer, K.R. Thampi, M. Gratzel, J. Catal. 146 (1994) 173–184.
[49] M. Marwood, R. Doepper, A. Renken, Appl. Catal. A 151 (1997) 223–246.
[50] P. Panagiotopoulou, D.I. Kondarides, X.E. Verykios, J. Phys. Chem. C 115 (2011) 1220–1230.